Thermodynamic stability of amorphous oxide films on metals: Application to aluminum oxide films on aluminum substrates

L. P. H. Jeurgens,[1,*] W. G. Sloof,[1,†] F. D. Tichelaar,[1] and E. J. Mittemeijer[1,2]
[1]*Laboratory of Materials Science, Delft University of Technology, 2628 AL Delft, The Netherlands*
[2]*Max Planck Institute for Metals Research, Seestrasse 92, 70174 Stuttgart, Germany*
(Received 4 November 1999)

It has been shown on a thermodynamic basis that an amorphous structure for an oxide film on its metal substrate can be more stable than the crystalline structure. The thermodynamic stability of a thin amorphous metal-oxide film on top of its single-crystal metal substrate has been modeled as a function of growth temperature, oxide-film thickness, and crystallographic orientation of the metal substrate. To this end, expressions have been derived for the estimation of the energies of the metal-substrate amorphous-oxide film interface and the metal-substrate crystalline-oxide film interface as a function of growth temperature, and crystallographic orientation of the substrate (including the effect of strain due to the lattice mismatch). It follows that, up to a certain critical thickness of the amorphous oxide film, the higher bulk Gibbs free energy of the amorphous oxide film, as compared to the corresponding crystalline oxide film, can be compensated for by the lower sum of the surface and interfacial energies. The predicted occurrence of an amorphous aluminum-oxide film on various crystallographic faces of aluminum agrees well with previous transmission electron microscopy observations.

I. INTRODUCTION

Upon exposure of a clean metal or semiconductor substrate to oxygen at relatively low temperatures (say <500 K), often a thin (thickness <10 nm) passivating amorphous oxide film is formed (this holds for, e.g., Si, Ta, Nb, Al, Ge, Cr, and Te), whereas at higher temperatures thicker films develop and the (resulting) structure of the corresponding oxide film is in most cases crystalline.[1–5] However, for metals such as Cu, Co, Fe, Ni, Mo, and Zn, low-temperature oxidation is known to proceed by the direct formation and (epitaxial) growth of a crystalline oxide,[3,4,6–9] and, upon oxidation of Si, an amorphous SiO_2 film forms even at temperatures as high as 1300 K.[3,5]

For all these oxides, the bulk Gibbs free energy of formation of the amorphous oxide is larger than that of the corresponding crystalline oxide. Hence, for relatively thick oxide films where the contribution of the surface and interfacial energies is small, the oxide formed on its metal (or semiconductor)[10] substrate is expected to be crystalline at all temperatures. As will be demonstrated in this paper, a crystalline structure need not occur for thin oxide films on their metal substrates, where the surface and interface energies can be the dominating contributions for the total Gibbs free energy of the oxide film on its metal substrate. As shown in recent work on the thermodynamics of solid-state amorphization,[11] the energy of the interface between an amorphous phase and a crystalline phase is in many cases lower than that of the corresponding crystalline-crystalline interface. This also holds for the oxide film formed on a clean metal substrate, as will be shown here. Moreover, the surface energy of the amorphous metal oxide is often lower than that of the corresponding crystalline metal oxide (cf. Ref. 12). Consequently, up to a certain critical oxide-film thickness, a thin amorphous metal-oxide film on its metal substrate can be the stable modification with respect to the corresponding crystalline metal-oxide film on the same substrate due to the relatively low surface and interfacial energies of the metal-substrate amorphous-oxide film system.

In this paper, first a general thermodynamic basis is presented for assessment of bulk, surface, and interfacial energies. At present, experimental values are usually not available for the interfacial energies of the metal-(semiconductor-) substrate amorphous-oxide film, and the corresponding metal- (semiconductor-) substrate crystalline-oxide film interfaces as a function of growth temperature and crystallographic orientation of the substrate. Therefore, expressions for these quantities are derived here on the basis of the ''macroscopic atom'' approach.[11,13–16]

The thermodynamic model is applied to the case of an aluminum-oxide film on the {111}, {110}, and {100} crystallographic faces of an aluminum substrate. In this case, the crystalline oxide γ-Al_2O_3 competes with the amorphous Al_2O_3 oxide.[1,17–20] The predictions, as obtained by application of the model to the Al-Al_2O_3 system, are compared with experimental data obtained by transmission electron microscopy.

II. BASIS OF THE THERMODYNAMICAL MODEL

Consider two situations for a homogeneous metal-oxide film MO_x of uniform thickness h on its single-crystal line metal substrate M. In Fig. 1(a) an *amorphous* oxide film, denoted by $\{MO_x\}$, with a uniform thickness $h_{\{MO_x\}}$ is on top of its single-crystal metal substrate, denoted by $\langle M\rangle$. In Fig. 1(b), on the other hand, a *crystalline* oxide film, denoted by $\langle MO_x\rangle$, with a uniform thickness $h_{\langle MO_x\rangle}$, is on top of the single-crystal metal substrate $\langle M\rangle$. The composition of the

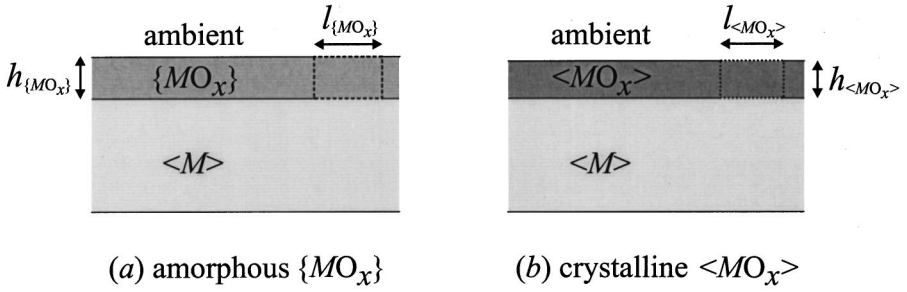

FIG. 1. Schematic drawing of a homogeneous MO_x oxide overlayer with uniform thickness on top of its single crystalline metal substrate $\langle M\rangle$. (a) displays an amorphous oxide film $\{MO_x\}$ with a uniform thickness $h_{\{MO_x\}}$ on the $\langle M\rangle$ substrate, while (b) shows a crystalline oxide-film $\langle MO_x\rangle$ of uniform thickness $h_{\{MO_x\}}$ on the $\langle M\rangle$ substrate (the braces $\{\}$ refer to the amorphous phase, and the brackets $\langle\,\rangle$ to the crystalline phase). The composition of $\{MO_x\}$ and $\langle MO_x\rangle$ is the same, and both films have been formed from the same molar quantity of oxygen on an identical metal substrate of $\langle M\rangle$. The two cells of volume $h_{\{MO_x\}}\times l^2_{\{MO_x\}}$ and $h_{\langle MO_x\rangle}\times l^2_{\langle MO_x\rangle}$, as indicated in (a) and (b) respectively, contain the same molar quantity of oxide. The ambient phase may be vacuum, a gas atmosphere, or an adsorbed layer.

amorphous and crystalline oxides is the same, and both films have been formed from the same molar quantity of oxygen on identical metal substrates $\langle M\rangle$. The thermodynamics of the $\langle M\rangle$-$\{MO_x\}$ and the $\langle M\rangle$-$\langle MO_x\rangle$ configuration will be described for cells of volume $h_{\{MO_x\}}\times l^2_{\{MO_x\}}$ and $h_{\langle MO_x\rangle}\times l^2_{\langle MO_x\rangle}$, respectively, as indicated in Figs. 1(a) and 1(b). Both cells contain the same molar quantity of oxide.

If an elastic strain exists within the amorphous $\{MO_x\}$ cell [cf. Fig. 1(a)], then the volume $V^{\rm str}_{\{MO_x\}}$ occupied by 1-mol $\{MO_x\}$ in the cell is related to the molar volume of strain-free $\{MO_x\}$, $V_{\{MO_x\}}$, by the fraction $\Omega_{\{MO_x\}}$: $V^{\rm str}_{\{MO_x\}}=\Omega_{\{MO_x\}}V_{\{MO_x\}}$. Analogously, if an elastic strain resides within the crystalline $\langle MO_x\rangle$ cell [cf. Fig. 1(b)], then $\Omega_{\langle MO_x\rangle}$ is defined by $V^{\rm str}_{\langle MO_x\rangle}=\Omega_{\langle MO_x\rangle}V_{\langle MO_x\rangle}$, where definitions for the quantities concerned are analogous to those given above.

Then, for the case of an amorphous oxide film $\{MO_x\}$ of uniform thickness $h_{\{MO_x\}}$ on the substrate $\langle M\rangle$, the total Gibbs free energy $G_{\rm am}$ of the cell considered [see Fig. 1(a)] is given by

$$G_{\rm am}=l^2_{\{MO_x\}}\left(h_{\{MO_x\}}\frac{G_{\{MO_x\}}}{\Omega_{\{MO_x\}}V_{\{MO_x\}}}+\gamma_{\{MO_x\}-\text{ambient}}+\gamma_{\langle M\rangle\text{-}\{MO_x\}}\right), \tag{1}$$

where $G_{\{MO_x\}}$ is the bulk Gibbs free energy of 1 mol of the amorphous oxide; $\gamma_{\{MO_x\}\text{-ambient}}$ represents the surface energy of the amorphous oxide; $\gamma_{\langle M\rangle\text{-}\{MO_x\}}$ is the energy of the interface between the metal substrate and the amorphous oxide; and $l_{\{MO_x\}}$ denotes the width and length of the cell, both parallel to the interface.

Analogously, for a crystalline layer $\langle MO_x\rangle$ of uniform thickness $h_{\langle MO_x\rangle}$ on the metal substrate $\langle M\rangle$, the total Gibbs free energy G_c of the cell considered [see Fig. 1(b)] is expressed by

$$G_c=l^2_{\langle MO_x\rangle}\left(h_{\langle MO_x\rangle}\frac{G_{\langle MO_x\rangle}}{\Omega_{\langle MO_x\rangle}V_{\langle MO_x\rangle}}+\gamma_{\langle MO_x\rangle\text{-ambient}}+\gamma_{\langle M\rangle\text{-}\langle MO_x\rangle}\right), \tag{2}$$

where $G_{\langle MO_x\rangle}$ is the molar bulk Gibbs free energy of the crystalline oxide; $\gamma_{\langle MO_x\rangle\text{-ambient}}$ represents the surface energy of the crystalline oxide; $\gamma_{\langle M\rangle\text{-}\langle MO_x\rangle}$ is the energy of the interface between the metal substrate and the crystalline oxide; and finally $l_{\langle MO_x\rangle}$ denotes the width and length of the cell, both parallel to the interface.

The amorphous oxide film $\{MO_x\}$ is stable with respect to the corresponding crystalline oxide film $\langle MO_x\rangle$, as long as the total Gibbs free energy $G_{\rm am}$ of the $\{MO_x\}$ cell in the crystalline-amorphous configuration, $\langle M\rangle$-$\{MO_x\}$, is lower than the total Gibbs free energy G_c of the corresponding $\langle MO_x\rangle$ cell in the crystalline-crystalline configuration, $\langle M\rangle$-$\langle MO_x\rangle$: $\Delta G\equiv G_{\rm am}-G_c<0$. To arrive at an explicit expression for ΔG, first the bulk energy terms in Eqs. (1) and (2) are considered; the interfacial energy terms are dealt with separately in Sec. III.

The Gibbs free energy of formation $\Delta G^f_{\{MO_x\}}$ of 1-mol $\{MO_x\}$ out of its elements in their stable configuration, for a given temperature and pressure, is defined as

$$\Delta G^f_{\{MO_x\}}\equiv G_{\{MO_x\}}-G_{\langle M\rangle}-\frac{x}{2}G_{O_2(g)}. \tag{3a}$$

Likewise, the Gibbs free energy of formation $\Delta G^f_{\langle MO_x\rangle}$ of one mole $\langle MO_x\rangle$ is given by

$$\Delta G^f_{\langle MO_x\rangle}\equiv G_{\langle MO_x\rangle}-G_{\langle M\rangle}-\frac{x}{2}G_{O_2(g)}. \tag{3b}$$

Because both cells are of the same composition and contain the same molar quantity of oxygen, it holds that

$$\frac{l^2_{\{MO_x\}}h_{\{MO_x\}}}{\Omega_{\{MO_x\}}V_{\{MO_x\}}}=\frac{l^2_{\langle MO_x\rangle}h_{\langle MO_x\rangle}}{\Omega_{\langle MO_x\rangle}V_{\langle MO_x\rangle}}. \tag{4a}$$

Now, defining χ as the ratio of the surface areas of the $\langle MO_x\rangle$ and $\{MO_x\}$ cells, i.e.,

$$\chi=\frac{l^2_{\langle MO_x\rangle}}{l^2_{\{MO_x\}}}, \tag{4b}$$

it follows from Eqs. (1)–(4b) that $\Delta G\equiv G_{\rm am}-G_c$ per *unit area* of the $\langle M\rangle$-$\{MO_x\}$ interface of the amorphous $\{MO_x\}$ cell can be expressed as

$$\Delta G=h_{\{MO_x\}}\left(\frac{\Delta G^f_{\{MO_x\}}-\Delta G^f_{\langle MO_x\rangle}}{\Omega_{\{MO_x\}}V_{\{MO_x\}}}\right)+\gamma_{\{MO_x\}\text{-ambient}}+\gamma_{\langle M\rangle\text{-}\{MO_x\}}-\chi(\gamma_{\langle MO_x\rangle\text{-ambient}}+\gamma_{\langle M\rangle\text{-}\langle MO_x\rangle}). \tag{5}$$

III. ENERGY OF METAL-SUBSTRATE OXIDE-FILM INTERFACES

In most cases, experimental values are not available for the energies between the metal substrate and the oxide film. In the following, expressions will be derived for these interfacial energies on the basis of the ''macroscopic atom'' approach.[11,13–16]

A. Energy of the crystalline-amorphous $\langle M\rangle$-$\{MO_x\}$ interface

To assess the energy of the interface between the crystalline metal substrate $\langle M\rangle$ and the amorphous oxide film $\{MO_x\}$, the interface between a crystalline solid (i.e., $\langle M\rangle$) and a configurationally frozen liquid (as a model for $\{MO_x\}$) is considered. Then, three contributions to the interfacial energy $\gamma_{\langle M\rangle\text{-}\{MO_x\}}$ can be recognized:[11,13,16]

$$\gamma_{\langle M\rangle\text{-}\{MO_x\}}=\gamma^{\rm interaction}_{\langle M\rangle\text{-}\{MO_x\}}+\gamma^{\rm entropy}_{\langle M\rangle\text{-}\{MO_x\}}+\gamma^{\rm enthalpy}_{\langle M\rangle\text{-}\{MO_x\}}. \tag{6}$$

It is assumed that, at the oxide-film growth temperature, mismatch strain does not occur in the amorphous oxide film (and the metal substrate) due to the relative large free volume[21,22] and the bond flexibility[2,23] of the amorphous structure, which make viscous flow in the oxide film easy.[2,21–26] Therefore, at the growth temperature, $\Omega_{\{MO_x\}}=1$ [cf. Eq. (5)]. It is noted that, even in the absence of viscous flow and with a large mismatch between the amorphous oxide film and its metal substrate, the strain in the amorphous oxide film (at the growth temperature) may be small.[24]

1. Interaction contribution to the $\langle M\rangle$-$\{MO_x\}$ interfacial energy

The interaction between the metal substrate $\langle M\rangle$ and the amorphous oxide film $\{MO_x\}$ across the $\langle M\rangle$-$\{MO_x\}$ interface can be subdivided into chemical and London–van der Waals interactions between (i) the M atoms of the metal substrate $\langle M\rangle$ and the O atoms of the oxide ($\gamma^{\rm interaction}_{\langle M\rangle\text{-O}}$), and (ii) the M atoms of the metal substrate $\langle M\rangle$ and the M atoms of the oxide ($\gamma^{\rm interaction}_{\langle M\rangle\text{-}M}$),[13,27,28] i.e.,

$$\gamma^{\rm interaction}_{\langle M\rangle\text{-}\{MO_x\}}=\gamma^{\rm interaction}_{\langle M\rangle\text{-O}}+\gamma^{\rm interaction}_{\langle M\rangle\text{-}M}. \tag{7a}$$

The metal-oxygen interaction energy $\gamma^{\rm interaction}_{\langle M\rangle\text{-O}}$ across the $\langle M\rangle$-$\{MO_x\}$ interface can be estimated from the enthalpy of mixing at infinite dilution of 1-mol O(g) atoms in $\langle M\rangle$, $\Delta H^{\infty}_{{\rm O}\,\langle M\rangle}$.[13,28,14] If the O atoms would be fully surrounded by M atoms, then $\Delta H^{\infty}_{{\rm O}\,\langle M\rangle}$ is the enthalpy increase per mol O(g) atoms in an infinitely diluted system. At the $\langle M\rangle$-$\{MO_x\}$ interface, only a fraction p of the total surface area of the O atomic cell is in contact with M atoms of the $\langle M\rangle$ substrate. Thus the metal-oxygen interaction energy $\gamma^{\rm interaction}_{\langle M\rangle\text{-O}}$ *per mol* O atoms at the interface equals $p\Delta H^{\infty}_{{\rm O\ in}\,\langle M\rangle}$. Then, if the molar interface area $A_{\{\rm O\}}$ is defined as the area of the $\langle M\rangle$-$\{MO_x\}$ interface containing 1-mol O atoms, the interaction energy $\gamma^{\rm interaction}_{\langle M\rangle\text{-O}}$ *per unit area* of the $\langle M\rangle$-$\{MO_x\}$ interface becomes

$$\gamma^{\rm interaction}_{\langle M\rangle\text{-O}}=\frac{p\Delta H^{\infty}_{{\rm O\ in}\,\langle M\rangle}}{A_{\{\rm O\}}}. \tag{7b}$$

The fraction p depends on the shape of the Wigner-Seitz cell of oxygen in $\{MO_x\}$, and can be taken, on average, as $p=\frac{1}{3}$, assuming a shape of the oxygen atomic cell between a cube ($p=\frac{1}{6}$) and a sphere ($p=\frac{1}{2}$) (cf. Refs. 11 and 13). For those metal-oxide systems for which the enthalpy of mixing at infinite dilution of 1-mol O(g) atoms in $\langle M\rangle$, i.e., $\Delta H^{\infty}_{{\rm O\ in}\,\langle M\rangle}$, is unknown, a value can be estimated from the following empirical relation between $\Delta H^{\infty}_{{\rm O\ in}\,\langle M\rangle}$ and the enthalpy of formation $\Delta H^f_{\langle MO_x\rangle}$ per mole O, as obtained from the data in Refs. 29–32:

$$\Delta H^{\infty}_{{\rm O\ in}\,\langle M\rangle}\cong 1.2\Delta H^f_{\langle MO_x\rangle}+1\times 10^5 \quad ({\rm J\,mol^{-1}\ O}). \tag{7c}$$

Since, for most metal-oxide systems, the metal-oxygen bond formation is strongly exothermic, the relatively large *negative* metal-oxygen interaction energy $\gamma^{\rm interaction}_{\langle M\rangle\text{-O}}$ is the dominant contribution to the interfacial energy $\gamma_{\langle M\rangle\text{-}\{MO_x\}}$. Thus the lowest interfacial energy $\gamma_{\langle M\rangle\text{-}\{MO_x\}}$ is achieved by maximizing the number of metal-oxygen bonds across the $\langle M\rangle$-$\{MO_x\}$ interface per unit area of the interface, resulting in a dense packing of the amorphous oxide at the interface. The value of $A_{\{\rm O\}}$ for an amorphous oxide film $\{MO_x\}$ on the different crystallographic faces of its metal substrate $\langle M\rangle$ in Eq. (7b) may therefore be approximated by taking it to be equal to the molar interface area $A_{\langle \rm O\rangle}$ at the most densely packed plane of the corresponding (unstrained) crystalline phase $\langle MO_x\rangle$.

The metal-metal interaction energy $\gamma^{\rm interaction}_{\langle M\rangle\text{-}M}$ across the $\langle M\rangle$-$\{MO_x\}$ interface between an M atom of the $\langle M\rangle$ substrate and an M atom of the amorphous oxide $\{MO_x\}$ [cf. Eq. (7a)] can be estimated analogously from the enthalpy of mixing at infinite dilution of 1-mol M atoms in an infinitely large reservoir of $\langle M\rangle$, $\Delta H^{\infty}_{{\rm M\ in}\,\{M\}}$. Since the enthalpy of solution of 1-mol M atoms in an infinitely large reservoir of $\langle M\rangle$, $\Delta H^{\infty}_{{\rm Min}\langle M\rangle}\equiv 0$, the metal-metal interaction energy across the $\langle M\rangle$-$\{MO_x\}$ interface, $\gamma^{\rm interaction}_{\langle M\rangle\text{-}M}=0$. However, for metal-oxide interfaces $\langle M^I\rangle$-$\{M^{II}{\rm O}_x\}$, where $M^I\neq M^{II}$, the M^I-M^{II} interaction energy $\gamma^{\rm interaction}_{\langle M^{II}\rangle\text{-}M^I}$ across the interface should, of course, not be neglected as, in general, the enthalpy of solution of M^{II} in an infinitely large reservoir of metal M^I, $\Delta H^{\infty}_{M^{II}\,{\rm in}\,M^I}\neq 0$.

2. Entropy contribution to the $\langle M\rangle$-$\{MO_x\}$ interfacial energy

The entropy contribution to the $\langle M\rangle$-$\{MO_x\}$ interfacial energy, $\gamma^{\text{entropy}}_{\langle M\rangle\text{-}\{MO_x\}}$, is ascribed to the *decrease* in configurational entropy of the amorphous $\{MO_x\}$ phase near the interface relative to that of bulk $\{MO_x\}$.[33–35] Due to the strong interaction between the crystalline metal substrate and the amorphous oxide film across the $\langle M\rangle$-$\{MO_x\}$ interface (cf. Sec. III A 1), ordering of the amorphous phase occurs near the $\langle M\rangle$-$\{MO_x\}$ interface. Because the structure of the crystalline metal substrate remains unaltered up to the interface, the (positive) entropy contribution to the $\langle M\rangle$-$\{MO_x\}$ interfacial energy is solely due to the decrease in entropy of the amorphous $\{MO_x\}$ phase near the interface.

The decrease of configurational entropy per mole $\{MO_x\}$, $\Delta S^{\text{deficient}}_{\{MO_x\}}$, i.e., the difference in entropy of $\{MO_x\}$ at the $\langle M\rangle$-$\{MO_x\}$ interface relative to that of bulk $\{MO_x\}$, is associated with the following contribution to the interfacial energy $\gamma_{\langle M\rangle\text{-}\{MO_x\}}$ per *unit area* interface,

$$\gamma^{\text{entropy}}_{\langle M\rangle\text{-}\{MO_x\}} = \frac{-T\Delta S^{\text{deficient}}_{\{MO_x\}}}{xA_{\{O\}}}, \tag{8a}$$

where the area occupied by 1-mol $\{MO_x\}$ at the interface follows from the molar interface area of O at the interface, $A_{\{O\}}$ (cf. Sec. III A 1), multiplied by x.

An (over)estimate for the entropy of the ordered $\{MO_x\}$ phase *at* the $\langle M\rangle$-$\{MO_x\}$ interface, $S^{\text{interface}}_{\{MO_x\}}$, is obtained by taking it to be equal to the entropy of the corresponding crystalline oxide of identical composition, $S_{\langle MO_x\rangle}$. Then the decrease in entropy of $\{MO_x\}$ at the interface relative to the entropy $S_{\{MO_x\}}$ of bulk $\{MO_x\}$ is given by $\Delta S^{\text{deficient}}_{\{MO_x\}} \cong S_{\langle MO_x\rangle} - S_{\{MO_x\}} < 0$.

Another estimate for $\Delta S^{\text{deficient}}_{\{MO_x\}}$ can be obtained on the basis of the structural model for the solid-liquid $\langle A\rangle$-$\{A\}$ interface, considered as an interface between a dense random packing of hard spheres (i.e., the liquid) and a close-packed crystal plane (i.e., the solid).[33,34] As demonstrated in Ref. 11 for the case of an amorphous binary alloy $\{AB\}$ in contact with a crystalline metal $\langle A\rangle$, the decrease in configurational entropy of $\{AB\}$ at the interface relative to that of bulk $\{AB\}$ is given by $0.904R\ \text{J K}^{-1}$ (R is the gas constant) per mole $\{AB\}$ at the $\langle A\rangle$-$\{AB\}$ interface. Accordingly, for the $\langle M\rangle$-$\{MO_x\}$ interface considered here, it then follows that

$$\gamma^{\text{entropy}}_{\langle M\rangle\text{-}\{MO_x\}} = \frac{0.904RT}{xA_{\{O\}}}. \tag{8b}$$

In the estimation of the entropy term $0.904R$ in Eq. (8b), the atoms of $\{MO_x\}$ are considered as equally sized hard spheres,[11,16,33,34] and therefore Eq. (8b) can only be considered as a crude estimate. In this paper, Eq. (8a) (with $\Delta S^{\text{deficient}}_{\{MO_x\}} \cong S_{\langle MO_x\rangle} - S_{\{MO_x\}}$; see above) will be used to estimate the entropy contribution.

3. Enthalpy contribution to the $\langle M\rangle$-$\{MO_x\}$ interfacial energy

The enthalpy contribution to the $\langle M\rangle$-$\{MO_x\}$ interfacial energy, $\gamma^{\text{enthalpy}}_{\langle M\rangle\text{-}\{MO_x\}}$, is ascribed to the *increase* in enthalpy of the M atoms of the $\langle M\rangle$ substrate *at* the interface relative to that of the M atoms in the bulk $\langle M\rangle$ substrate.[11,13,16,35] Because the interface between the crystalline substrate $\langle M\rangle$ and the amorphous oxide film $\{MO_x\}$ is considered as a crystalline-liquid rather than a crystalline-crystalline type of interface (cf. Sec. III A), the M atoms of the crystalline substrate $\langle M\rangle$ at the interface will be increased in enthalpy relative to that of bulk $\langle M\rangle$ due to the liquid type of bonding with the atoms of $\{MO_x\}$ at the $\langle M\rangle$-$\{MO_x\}$ interface.[11,13,16,35] If the enthalpy increase of the M atoms of $\langle M\rangle$ at the $\langle M\rangle$-$\{MO_x\}$ interface is taken to be the same as the enthalpy increase of the M atoms of the $\langle M\rangle$ substrate in contact with its amorphous phase $\{M\}$, then the enthalpy increase of the M atoms of the crystalline substrate $\langle M\rangle$ *at* the $\langle M\rangle$-$\{MO_x\}$ interface relative to that of bulk $\langle M\rangle$ will be proportional to the enthalpy of fusion of $\langle M\rangle$, $H^{\text{fuse}}_{\langle M\rangle}$.[11,13,16,35]

Since, at the interface, only a fraction p of the total surface area of the atomic $\langle M\rangle$ cell is in contact with the amorphous $\{MO_x\}$ phase, the enthalpy increase of one mole $\langle M\rangle$ atoms in the first atomic layer of the $\langle M\rangle$ substrate at the $\langle M\rangle$-$\{MO_x\}$ interface is estimated by $pH^{\text{fuse}}_{\langle M\rangle}$ (cf. Refs. 11, 13, 16, and 35). Now the enthalpy contribution $\gamma^{\text{enthalpy}}_{\langle M\rangle\text{-}\{MO_x\}}$ to the total $\langle M\rangle$-$\{MO_x\}$ interfacial energy per *unit area* interface is obtained by dividing $pH^{\text{fuse}}_{\langle M\rangle}$ by the area $A_{\langle M\rangle}$ occupied by 1-mol M atoms of the $\langle M\rangle$ substrate at the interface, i.e.,

$$\gamma^{\text{enthalpy}}_{\langle M\rangle\text{-}\{MO_x\}} = \frac{pH^{\text{fuse}}_{\langle M\rangle}}{A_{\langle M\rangle}}. \tag{9}$$

For a given crystallographic orientation of the $\langle M\rangle$ substrate, the molar interface area $A_{\langle M\rangle}$ can be calculated if the lattice parameter and the crystal structure of $\langle M\rangle$ are known.[36] The fraction p can be taken, on average, as $p = \frac{1}{3}$ (cf. Sec. III A 1).

4. Expression for the $\langle M\rangle$-$\{MO_x\}$ interfacial energy

Substitution of Eqs. (7b), (8a), and (9) into Eq. (6) finally leads to the following expression for the interfacial energy $\gamma_{\langle M\rangle\text{-}\{MO_x\}}$:

$$\gamma_{\langle M\rangle\text{-}\{MO_x\}} = \frac{p\Delta H^{\infty}_{\text{O in }\langle M\rangle}}{A_{\{O\}}} + \frac{-T\Delta S^{\text{deficient}}_{\{MO_x\}}}{xA_{\{O\}}} + \frac{pH^{\text{fuse}}_{\langle M\rangle}}{A_{\langle M\rangle}}. \tag{10}$$

B. Energy of the crystalline-crystalline $\langle M\rangle$-$\langle MO_x\rangle$ interface

The energy $\gamma_{\langle M\rangle\text{-}\langle MO_x\rangle}$ of the interface between the crystalline metal substrate $\langle M\rangle$ and the crystalline oxide $\langle MO_x\rangle$ is the resultant of a chemical and a structural term.[11,13,14,16,37] As for the crystalline-amorphous $\langle M\rangle$-$\{MO_x\}$ interface, the chemical term is related to the interaction between the atoms of $\langle M\rangle$ and $\langle MO_x\rangle$ across the interface, whereas the structural term is related to the strain induced by the mismatch at the interface between the two adjacent crystalline phases $\langle M\rangle$ and $\langle MO_x\rangle$, i.e.,

$$\gamma_{\langle M\rangle\text{-}\langle MO_x\rangle} = \gamma^{\text{interaction}}_{\langle M\rangle\text{-}\langle MO_x\rangle} + \gamma^{\text{mismatch}}_{\langle M\rangle\text{-}\langle MO_x\rangle}. \tag{11}$$

1. Interaction contribution to the $\langle M\rangle$-$\langle MO_x\rangle$ interfacial energy

Following the treatment given in Sec. III A 1 for the interaction energy across the crystalline-amorphous $\langle M\rangle$-$\{MO_x\}$ interface, the interaction energy $\gamma^{\text{interaction}}_{\langle M\rangle\text{-}\langle MO_x\rangle}$ across the corresponding crystalline-crystalline $\langle M\rangle$-$\langle MO_x\rangle$ interface is expressed by

$$\gamma^{\text{interaction}}_{\langle M\rangle\text{-}\langle MO_x\rangle}=\frac{p\Delta H^{\infty}_{\text{O in }\langle M\rangle}}{A_{\langle O\rangle}}. \tag{12}$$

Note that for a strained oxide film $\langle MO_x\rangle$ on its metal substrate $\langle M\rangle$, the correct molar interface area of oxygen $A_{\langle O\rangle}$, i.e. the area occupied by 1-mol O atoms of $\langle MO_x\rangle$ at the $\langle M\rangle$-$\langle MO_x\rangle$ interface, is calculated from the strained lattice spacing of $\langle MO_x\rangle$ *at* the interface (see Sec. IV C).

2. Mismatch contribution to $\langle M\rangle$-$\langle MO_x\rangle$ interfacial energy

Besides the relatively large negative contribution of the metal-oxide interaction energy $\gamma^{\text{interaction}}_{\langle M\rangle\text{-}\langle MO_x\rangle}$, the $\langle M\rangle$-$\langle MO_x\rangle$ interfacial energy $\gamma_{\langle M\rangle\text{-}\langle MO_x\rangle}$ also contains an additive positive energy contribution $\gamma^{\text{mismatch}}_{\langle M\rangle\text{-}\langle MO_x\rangle}$ corresponding to the strain induced by the mismatch at the interface between the two adjacent crystalline phases $\langle M\rangle$ and $\langle MO_x\rangle$. In the case considered here, i.e., the formation of a thin crystalline $\langle MO_x\rangle$ film on its metal substrate $\langle M\rangle$, a coherent $\langle M\rangle$-$\langle MO_x\rangle$ interface may occur as a result of epitaxial growth.[1,3,4,6–9,17–20,38] In such a case the mismatch between the adjacent lattices of the two crystalline phases is accommodated by elastic deformation. Generally, the mismatch in the boundary is characterized by the mismatch values in two directions within the boundary. One such mismatch f can be defined by[39,40]

$$f=\frac{d^{hkl}_{\langle M\rangle}-d^{HKL}_{\langle MO_x\rangle}}{d^{HKL}_{\langle MO_x\rangle}}, \tag{13a}$$

where $d^{HKL}_{\langle MO_x\rangle}$ and $d^{hkl}_{\langle M\rangle}$ represent the unstrained lattice spacings in the direction concerned of the (hkl) and (HKL) lattice planes perpendicular to the boundary of the $\langle M\rangle$ lattice and $\langle MO_x\rangle$ lattice, respectively. The unstrained lattice spacings of both lattices depend on temperature T according to

$$d^{hkl}_{\langle M\rangle}=d^{hkl,0}_{\langle M\rangle}(1+\alpha^{hkl}_{\langle M\rangle}\Delta T) \tag{13b}$$

and

$$d^{HKL}_{\langle MO_x\rangle}=d^{HKL,0}_{\langle MO_x\rangle}(1+\alpha^{HKL}_{\langle MO_x\rangle}\Delta T) \tag{13c}$$

where $d^{hkl,0}_{\langle M\rangle}$ and $d^{HKL,0}_{\langle MO_x\rangle}$ are the unstrained lattice spacings at the reference temperature T_0, $\alpha^{hkl}_{\langle M\rangle}$ and $\alpha^{HKL}_{\langle MO_x\rangle}$ denote the coefficients of linear thermal expansion of $\langle M\rangle$ and $\langle MO_x\rangle$, respectively, and $\Delta T=(T-T_0)$.

Because the epitaxial oxide film is very thin as compared with the metal substrate, all mismatch between the oxide film and the substrate will be accommodated fully elastically by the oxide film, and thus the strain in the oxide film in the direction pertaining to Eq. (13a) in a plane parallel to the interface, $\varepsilon_{\parallel}$, satisfies $\varepsilon_{\parallel}=f$ [cf. Eq. (13a)]. It should be noted that here the mismatch energy in the system is assigned to the $\langle M\rangle$-$\langle MO_x\rangle$ interfacial energy instead of the bulk Gibbs free energy of the oxide film; this choice has no effect on the outcome of the model calculations.

Thus the contribution of the mismatch strain to the interfacial energy [see Eq. (11)] is obtained as the elastic strain energy stored in the oxide film per unit area of the interface between the $\langle MO_x\rangle$ film and the metal substrate $\langle M\rangle$.[40] Then, for those cases where the mismatch f and thus the strain $\varepsilon_{\parallel}$ is independent of the direction within the plane parallel to the $\langle M\rangle$-$\langle MO_x\rangle$ interface (e.g., the $\langle$Al$\rangle$-$\langle\gamma$-$Al_2O_3\rangle$ interfaces considered in Sec. IV C), the contribution of the mismatch energy to the interfacial energy $\gamma_{\langle M\rangle\text{-}\langle MO_x\rangle}$ equals[40]

$$\gamma^{\text{mismatch}}_{\langle M\rangle\text{-}\langle MO_x\rangle}=h_{\langle MO_x\rangle}\left(\frac{E}{1-\nu}\right)\varepsilon^2_{\parallel}, \tag{13d}$$

where $h_{\langle MO_x\rangle}$ is the thickness of the $\langle MO_x\rangle$ film and ν and E denote the Poisson's ratio and the Young's modulus of $\langle MO_x\rangle$, respectively.

In principle part of the mismatch f may be compensated by plastic deformation. For plastic deformation to occur the mismatch and the oxide-film thickness must exceed critical values that increase with increasing bonding strength across the interface.[39,40] For an epitaxial $Ge_{0.25}Si_{0.75}$ film on a Si substrate, where the lattice mismatch $f=0.01$, a critical thickness of 16.3 nm was calculated.[44] Most $\langle M\rangle$-$\langle MO_x\rangle$ systems have lattice mismatches $f=0.02-0.07$ (cf. Refs. 1 and 6–8), and then up to an oxide-film thickness of, say, 5–10 nm, plastic deformation is considered not to play a role here (cf. Frank-van der Merwe theory; cf. Refs. 39, 40, and 45).

3. Expression for the $\langle M\rangle$-$\langle MO_x\rangle$ interfacial energy

Substitution of Eqs. (12) and (13d) into Eq. (11) finally leads to the following expression for the interfacial energy $\gamma_{\langle M\rangle\text{-}\langle MO_x\rangle}$:

$$\gamma_{\langle M\rangle\text{-}\langle MO_x\rangle}=\frac{p\Delta H^{\infty}_{\text{O in }\langle M\rangle}}{A_{\langle O\rangle}}+h_{\langle MO_x\rangle}\left(\frac{E}{1-\nu}\right)\varepsilon^2_{\parallel}. \tag{14}$$

IV. THERMODYNAMICS OF AMORPHOUS AND CRYSTALLINE ALUMINUM-OXIDE FILMS ON ALUMINUM SUBSTRATES

The thermodynamic model developed in Secs. II and III will be applied to the case of aluminum-oxide films on the {111}, {110}, and {100} crystallographic faces of an aluminum substrate. Such an oxide film can be produced by e.g., dry, thermal oxidation of a clean Al substrate. The crystalline oxide competing with the amorphous oxide $\{Al_2O_3\}$ of the same composition is γ-Al_2O_3.[1,17–20]

First the difference in bulk, surface, and interfacial energies of the amorphous $\{Al_2O_3\}$ cell on the $\langle$Al$\rangle$ substrate and the corresponding crystalline $\langle\gamma$-$Al_2O_3\rangle$ cell on the same substrate will be discussed. Then the stability of the oxide films is discussed as a function of growth temperature, oxide-film thickness, and crystallographic orientation of the $\langle$Al$\rangle$ substrate.

TABLE I. Some physical data of the Al-Al_2O_3 system at a standard state pressure $p_0 = 1 \times 10^5$ Pa ($T_0 = 298.15$ K, and N is Avogradro's number).

Name	Value		Unit	Ref.
coefficients of linear thermal expansion	$\alpha(T) = a + b\Delta T + c\Delta T^2$ ($T_0 \leqslant T \leqslant 900$ K)		K^{-1}	
	$\langle Al \rangle$:	$a = 2.3889 \times 10^{-5}$	K^{-1}	47
		$b = -1.1162 \times 10^{-9}$	K^{-2}	
		$c = 2.1757 \times 10^{-11}$	K^{-3}	
	$\langle \gamma\text{-}Al_2O_3 \rangle$:	a=2.6068×10−6	K^{-1}	48
		$b = 1.1499 \times 10^{-8}$	K^{-2}	
		$c = 0$	K^{-3}	
unstrained lattice parameters of the unit cells at T_0	$a^0_{\langle Al \rangle}$	$= 4.0494 \times 10^{-10}$	m	42
	$a^0_{\langle \gamma\text{-}Al_2O_3 \rangle}$	$= 7.924 \times 10^{-10}$	m	43
molar volumes at T_0	$V^0_{\langle Al \rangle}$	$= 1.00 \times 10^{-5}$	$m^3\,mole^{-1}$	
	$V^0_{\langle \gamma\text{-}Al_2O_3 \rangle}$	$= 2.81 \times 10^{-5}$	$m^3\,mole^{-1}$	
	$V^0_{\{Al_2O_3\}}$	$= 3.19 \times 10^{-5}$	$m^3\,mole^{-1}$	49
molar interface areas of $\langle Al \rangle$	{111}:	$A_{\langle Al \rangle} = \frac{1}{4}\sqrt{2}a^2_{\langle Al \rangle}N$	$m^2\,mole^{-1}$	
	{110}:	$A_{\langle Al \rangle} = \frac{1}{2}\sqrt{3}a^2_{\langle Al \rangle}N$	$m^2\,mole^{-1}$	
	{100}:	$A_{\langle Al \rangle} = \frac{1}{2}a^2_{\langle Al \rangle}N$	$m^2\,mole^{-1}$	
O molar interface area of $\{Al_2O_3\}$	$A_{\{O\}} = \frac{1}{4}\sqrt{2}\left(\frac{1}{2}a_{\langle \gamma\text{-}Al_2O_3 \rangle}\right)^2 N$		$m^2\,mole^{-1}$	
Poisson's ratio of $\langle \gamma\text{-}Al_2O_3 \rangle$	$\nu = 0.24(\pm 0.02)$			50
Young's modulus of $\langle \gamma\text{-}Al_2O_3 \rangle$	$E = 2.53 \times 10^{11}(\pm 0.22 \times 10^{11})$		$N\,m^{-2}$	50

A. Difference in bulk energy of $\{Al_2O_3\}$ and $\langle \gamma\text{-}Al_2O_3 \rangle$

The values for the Gibbs free energy of formation,[46] the enthalpy of formation and the entropy of γ-Al_2O_3 and the configurationally frozen Al_2O_3 liquid (as model for amorphous $\{Al_2O_3\}$; see Sec. III A) are taken from Ref. 29. The molar volumes of the cubic phases $\langle Al \rangle$ and $\langle \gamma\text{-}Al_2O_3 \rangle$ (cf. Ref. 41) from $T_0 = 298.15$ K up to the melting point of $\langle Al \rangle$ at 933.45 K are calculated from $V(T) = V^0(1 + \alpha\Delta T)^3$, where α and V^0 denote the coefficient of linear thermal expansion at $T > T_0$ and the molar volume at T_0, respectively (see Table I). The coefficient of linear thermal expansion of $\{Al_2O_3\}$ is taken to be the same as that of $\langle \gamma\text{-}Al_2O_3 \rangle$. All values used for the calculation were taken at a standard state pressure of $p_0 = 1 \times 10^5$ Pa; it is noted that the effect of pressure on the *difference*, in bulk, surface and interfacial energies of $\{Al_2O_3\}$ and $\langle \gamma\text{-}Al_2O_3 \rangle$ can be neglected (see Sec. V).

The calculated difference in the bulk Gibbs free energy of the $\{Al_2O_3\}$ cell and the corresponding $\langle \gamma\text{-}Al_2O_3 \rangle$ cell per unit area of the $\langle Al \rangle$-$\{Al_2O_3\}$ interface [cf. Eq. (5) in Sec. II] is plotted in Fig. 2 as a function of $h_{\{Al_2O_3\}}$ (i.e., the thickness of the amorphous oxide film) for both T_0 and $T = 900$ K. The crystalline $\langle \gamma\text{-}Al_2O_3 \rangle$ cell is of course thermodynamically more stable than the amorphous $\{Al_2O_3\}$ cell when only considering the difference in bulk energy of the two phases. Since at the melting temperature of γ-Al_2O_3 it holds that $\Delta G^f_{\langle \gamma\text{-}Al_2O_3 \rangle} \equiv \Delta Gf^f_{\{Al_2O_3\}}$, the $\{Al_2O_3\}$ cell becomes relatively more stable at higher T (see Fig. 2).

B. Difference in surface energy of $\{Al_2O_3\}$ and $\langle \gamma\text{-}Al_2O_3 \rangle$

The only values reported in the literature for the surface energies of the {111}, {110}, and {100} crystallographic faces of γ-Al_2O_3 are theoretical ones obtained from molecular-dynamics simulations pertaining to 300 K of the corresponding relaxed and unrelaxed surfaces of γ-Al_2O_3 in contact with vacuum (i.e., γ-$_{\langle \gamma\text{-}Al_2O_3 \rangle\text{-vac}}$).[12] For Al_2O_3 films grown

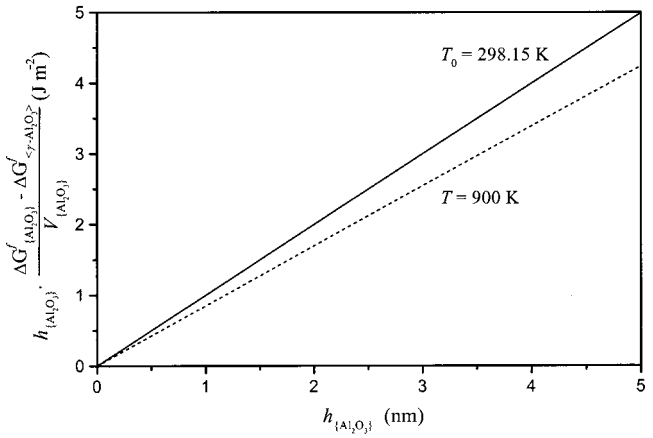

FIG. 2. Difference in bulk Gibbs free energy of the amorphous $\{Al_2O_3\}$ cell and the corresponding crystalline $\langle \gamma\text{-}Al_2O_3 \rangle$ cell per unit area of the $\langle Al \rangle$-$\{Al_2O_3\}$ interface [cf. Eq. (5) in Sec. II] as a function of $h_{\{Al_2O_3\}}$ (i.e., the thickness of the amorphous oxide film) at both $T_0 = 298.15$ K and $T = 900$ K. Note that $\Omega_{\{Al_2O_3\}} = 1$ in Eq. (5) of Sec. II [cf. Sec. III A below Eq. (6) and Ref. 26].

on Al substrates in an oxygen ambient e.g., by dry thermal oxidation, the surface energies of the oxygen-terminated surfaces of γ-Al_2O_3 are adopted. Many crystalline metal oxides lower their surface energy by surface relaxation,[12,51] and then the relaxed surface energies need to be considered.

According to Ref. 12, $\gamma_{\langle\{110\}\gamma\text{-}Al_2O_3\rangle\text{-vac}} = 2.54\,J\,m^{-2}$ and $\gamma_{\langle\{100\}\gamma\text{-}Al_2O_3\rangle\text{-vac}} = 1.94\,J\,m^{-2}$ for the relaxed oxygen-terminated {110} and {100} crystallographic faces of γ-Al_2O_3 at $T = 300$ K, respectively. These theoretical values can be compared with the experimental value of $\gamma_{\langle\gamma\text{-}Al_2O_3\rangle\text{-vac}} = 1.67\,J\,m^{-2}$ determined for nanocrystalline γ-Al_2O_3 at T_0 (Ref. 52). For the linear temperature dependencies of the surface energies of the {110} and {100} crystallographic faces of γ-Al_2O_3, an average linear temperature coefficient of $-0.50\times10^{-3}\,J\,m^{-2}\,K^{-1}$ is taken as estimated from the experimental and theoretical values of $\gamma_{\langle\gamma\text{-}Al_2O_3\rangle\text{-vac}}$ at various temperatures reported in Refs. 52 and 53, i.e., $\gamma_{\langle\gamma\text{-}Al_2O_3\rangle\text{-vac}}(T) = \gamma_{\langle\gamma\text{-}Al_2O_3\rangle\text{-vac}}(T_0) - 0.50\times10^{-3}(T - T_0)$.

Data for the oxygen-terminated {111} crystallographic face of γ-Al_2O_3 are not available. Only the two possible aluminum-terminated {111} γ-Al_2O_3 surfaces were simulated, which both became amorphous upon relaxation as a result of surface reconstruction.[12] Therefore, the resulting value for the surface energy of the two relaxed aluminum-terminated {111} crystallographic faces of γ-Al_2O_3, at 300 K of 0.88 $J\,m^{-2}$ (see Ref. 12), in fact represents the value for the surface energy of $\{Al_2O_3\}$ at 300 K, i.e., $\gamma_{\{Al_2O_3\}\text{-vac}}$ $(= \gamma_{\langle\{111\}\gamma\text{-}Al_2O_3\rangle\text{-vac}}) = 0.88\,J\,m^{-2}$. Taking for the linear temperature coefficient of $\gamma_{\{Al_2O_3\}\text{-vac}}$ (see above), the value experimentally determined for liquid Al_2O_3, i.e., -0.187×10^{-3} (Ref. 54), then the calculated theoretical value of $\gamma_{\{Al_2O_3\}\text{-vac}}$ at the melting point $T_m = 2325$ K becomes 0.50 $J\,m^{-2}$, which agrees well with the corresponding experimental value of 0.57 $J\,m^{-2}$ for the surface energy of liquid Al_2O_3 at T_m.[54]

It may be assumed that, as for the relaxed Al-terminated $\{111\}\,\gamma$-Al_2O_3 surfaces, the relaxed O-terminated {111} surface is also amorphous due to surface reconstruction, and therefore also has a surface energy at T_0 of 0.88 $J\,m^{-2}$ (see above). Then it can be concluded from the above data that the surface energy of the relaxed O-terminated surfaces of γ-Al_2O_3 increases with decreasing atomic density at the (unrelaxed) γ-Al_2O_3 surface: $\gamma_{\langle\{111\}\gamma\text{-}Al_2O_3\rangle\text{-vac}} < \gamma_{\langle\{100\}\gamma\text{-}Al_2O_3\rangle\text{-vac}} < \gamma_{\langle\{110\}\gamma\text{-}Al_2O_3\rangle\text{-vac}}$

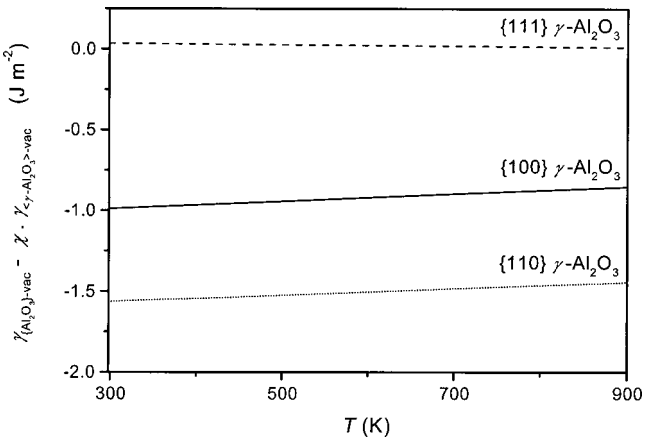

FIG. 3. Difference in surface energy of the amorphous $\{Al_2O_3\}$ cell and the corresponding crystalline $\langle\gamma$-$Al_2O_3\rangle$ cell per unit area of the $\{Al_2O_3\}$ surface [cf. Eq. (5)], as a function of T for the {111}, {110}, and {100} crystallographic faces of γ-Al_2O_3. The ratio χ relates the surface areas of the $\{Al_2O_3\}$ cell and the strained $\langle\gamma$-$Al_2O_3\rangle$ cell, and has been calculated using Eq. (A2) in the Appendix.

The calculated difference in surface energy between $\{Al_2O_3\}$ and $\langle\gamma$-$Al_2O_3\rangle$ per unit area of the $\{Al_2O_3\}$ surface [cf. Eq. (5)] is plotted in Fig. 3 as a function of T for the three different crystallographic faces of γ-Al_2O_3 considered. The ratio χ relating the surface areas of the (unstrained) $\{Al_2O_3\}$ cell [cf. Sec. III A below Eq. (6), and Ref. 26] and the (strained) $\langle\gamma$-$Al_2O_3\rangle$ cell [see Eq. (4b) in Sec. II] was calculated using Eq. (A2) in the Appendix. As follows from Fig. 3, the surface energy of amorphous $\{Al_2O_3\}$ is smaller than those of the {110} and {100} surfaces of $\langle\gamma$-$Al_2O_3\rangle$ (at T_0, 1.57 and 0.99 $J\,m^{-2}$ smaller, respectively), whereas it is slightly larger than that of the {111} surface of $\langle\gamma$-$Al_2O_3\rangle$ (this difference would be zero if χ equals 1; cf. the Appendix). The temperature dependencies of the differences in surface energies are negligible.

C. Difference in energy of $\langle$Al$\rangle$-$\{Al_2O_3\}$ and $\langle$Al$\rangle$-$\langle\gamma$-$Al_2O_3\rangle$ interfaces

The value of the interfacial energy of the crystalline-amorphous $\langle$Al$\rangle$-$\{Al_2O_3\}$ interface (i.e., $\gamma_{\langle Al\rangle\text{-}\{Al_2O_3\}}$) is the sum of the interaction, entropy, and enthalpy contributions (see Sec. III A). Values for these separate energy contributions for the $\langle$Al$\rangle$-$\{Al_2O_3\}$ interface (calculated as indicated

TABLE II. Interfacial energy of the crystalline-amorphous $\langle$Al$\rangle$-$\{Al_2O_3\}$ interface, as calculated using Eq. (10) given in Sec. III A 4, for an $\{Al_2O_3\}$ oxide film on the {111}, {110}, and {100} crystallographic faces of an $\langle$Al$\rangle$ substrate at different growth temperatures T. The interaction, entropy, and enthalpy contributions to the interfacial energy $\gamma_{\langle Al\rangle\text{-}\{Al_2O_3\}}$ were obtained using Eqs. (7b), (8a), and (9) given in Sec. III, respectively. Data used were taken from Ref. 29 and Table I.

T (K)	$\gamma^{\text{interaction}}_{\langle Al\rangle\text{-}\{Al_2O_3\}}$ ($J\,m^{-2}$)	$\gamma^{\text{entropy}}_{\langle Al\rangle\text{-}\{Al_2O_3\}}$ ($J\,m^{-2}$)	$\gamma^{\text{enthalpy}}_{\langle Al\rangle\text{-}\{Al_2O_3\}}$ ($J\,m^{-2}$)			$\gamma_{\langle Al\rangle\text{-}\{Al_2O_3\}}$ ($J\,m^{-2}$)		
			{111}	{110}	{100}	{111}	{110}	{100}
298	−4.583	+0.036	+0.083	+0.051	+0.072	−4.463	−4.495	−4.474
600	−4.560	+0.057	+0.082	+0.050	+0.071	−4.420	−4.452	−4.431
900	−4.511	+0.069	+0.080	+0.049	+0.070	−4.361	−4.393	−4.372

TABLE III. Interfacial energy of the crystalline-crystalline $\langle Al\rangle$-$\langle \gamma\text{-}Al_2O_3\rangle$ interface as calculated using Eq. (14) in Sec. III B 3 for an (epitaxial) $\langle \gamma\text{-}Al_2O_3\rangle$ oxide film on the {111}, {110}, and {100} crystallographic faces of an $\langle Al\rangle$ substrate at different growth temperatures T and for various film thicknesses $h_{\langle \gamma\text{-}Al_2O_3\rangle}$. The interaction and mismatch contributions to the interfacial energy $\gamma_{\langle Al\rangle\text{-}\langle \gamma\text{-}Al_2O_3\rangle}$ were obtained using Eqs. (12) and (13d), respectively. Data used were taken from Ref. 29 and Table I.

T (K)	$h_{\langle \gamma\text{-}Al_2O_3\rangle}$ (nm)	$\gamma^{\text{interaction}}_{\langle Al\rangle\text{-}\langle \gamma\text{-}Al_2O_3\rangle}$ (J m^{-2}) {111}	{110}	{100}	$\gamma^{\text{mismatch}}_{\langle Al\rangle\text{-}\langle \gamma\text{-}Al_2O_3\rangle}$ (J m^{-2})	$\gamma_{\langle Al\rangle\text{-}\langle \gamma\text{-}Al_2O_3\rangle}$ (J m^{-2}) {111}	{110}	{100}
298	1	−4.387	−2.690	−3.799	+0.162	−4.225	−2.528	−3.637
	3				+0.486	−3.901	−2.204	−3.313
	5				+0.810	−3.577	−1.880	−2.989
600	1	−4.315	−2.640	−3.736	+0.262	−4.053	−2.378	−3.475
	3				+0.786	−3.529	−1.854	−2.951
	5				+1.310	−3.005	−1.330	−2.427
900	1	−4.209	−2.580	−3.645	+0.414	−3.795	−2.166	−3.231
	3				+1.241	−2.968	−1.339	−2.404
	5				+2.068	−2.141	−0.512	−1.577

in Sec. III A) and the resulting value of the interfacial energy $\gamma_{\langle Al\rangle\text{-}\{Al_2O_3\}}$ are reported in Table II for the three crystallographic faces of $\langle Al\rangle$ considered. The value of the interfacial energy $\gamma_{\langle Al\rangle\text{-}\{Al_2O_3\}}$ is dominated by the negative contribution of the Al-O interaction energy [cf. the discussion below Eq. (7c) in Sec. III A 1]. Therefore, $\gamma_{\langle Al\rangle\text{-}\{Al_2O_3\}}<0$, and its value only slightly increases (i.e., becomes less negative) with increasing growth temperature T due to the small increases of both the interaction energy contribution and the entropy energy contribution with increasing T. As an approximation for the molar interface area of oxygen of the amorphous oxide at the three $\langle Al\rangle$-$\{Al_2O_3\}$ interfaces considered, the molar interface area of oxygen in the most densely packed plane of $\langle \gamma\text{-}Al_2O_3\rangle$, i.e. the {111} γ-Al_2O_3 plane, has been taken (see Table I), as discussed below Eq. (7c) in Sec. III A 1. Consequently, only the relatively small positive enthalpy contribution to the interfacial energy depends on the crystallographic orientation of the $\langle Al\rangle$ substrate [cf. Table II and Eq. (9)]. It can be concluded that the interfacial energy $\gamma_{\langle Al\rangle\text{-}\{Al_2O_3\}}<0$, and that its value is approximately independent of both the growth temperature and the crystallographic orientation of the $\langle Al\rangle$ substrate (see Table II).

The value of the interfacial energy of the crystalline-crystalline $\langle Al\rangle$-$\langle \gamma\text{-}Al_2O_3\rangle$ interface (i.e., $\gamma_{\langle Al\rangle\text{-}\langle \gamma\text{-}Al_2O_3\rangle}$) is the sum of the interaction and the mismatch contributions (see Sec. III B). For all three crystallographic faces of $\langle Al\rangle$ considered,[55] the orientation relationship between $\langle Al\rangle$ and $\langle \gamma\text{-}Al_2O_3\rangle$ is given by[1,17-20] $(111)_{Al}\|(111)_{\gamma\text{-}Al_2O_3}$ and $[110]_A\|[110]_{\gamma\text{-}Al_2O_3}$. From the crystallographic structure of $\langle Al\rangle$ and $\langle \gamma\text{-}Al_2O_3\rangle$ (see Ref. 41), it then follows that, at the oxide-film growth temperature, the ''growth'' mismatch f (see Sec. III B 2) in all directions parallel to the $\langle Al\rangle$-$\langle \gamma\text{-}Al_2O_3\rangle$ interface is the same for the three crystallographic faces of $\langle Al\rangle$ considered, and equals

$$f=\frac{2a_{\langle Al\rangle}}{a_{\langle \gamma-Al_2O_3\rangle}}-1, \tag{15}$$

where $a_{\langle Al\rangle}$ and $a_{\langle \gamma\text{-}Al_2O_3\rangle}$, are the unstrained lattice parameters of the Al and γ-Al_2O_3 unit cells[41] at the growth temperature T, as calculated according to Eqs. (13b) and (13c) (using the values reported in Table I), respectively. Since $f>0$ and all growth mismatch is accommodated fully elastically by the thin (epitaxial) $\langle \gamma\text{-}Al_2O_3\rangle$ film (see Sec. III B 2), a tensile strain $\varepsilon_{\|}$ of value f resides within the oxide film parallel to the $\langle Al\rangle$-$\langle \gamma\text{-}Al_2O_3\rangle$ interface. The contribution of the mismatch energy to the interfacial energy $\gamma_{\langle Al\rangle\text{-}\langle \gamma\text{-}Al_2O_3\rangle}$ can be calculated using Eq. (13d) in Sec. II B 2.

The contribution of the Al-O interaction energy to the interfacial energy $\gamma_{\langle Al\rangle\text{-}\langle \gamma\text{-}Al_2O_3\rangle}$ can be calculated applying Eq. (12) in Sec. III B 1. To this end, the molar interface area $A_{\langle O\rangle}$ must be calculated from the *strained* lattice parameter of $\langle \gamma\text{-}Al_2O_3\rangle$ at the interface (cf. Sec. III B 1). All mismatch strain is accommodated fully elastically by the thin $\langle \gamma\text{-}Al_2O_3\rangle$ film (see above), and thus [cf. Eq. (15)] the strained lattice parameter of $\langle \gamma\text{-}Al_2O_3\rangle$ is equal to twice the *unstrained* lattice parameter of $\langle Al\rangle$ (see also Ref. 41). From the crystallographic structure and composition of the $\langle Al\rangle$ and $\langle \gamma\text{-}Al_2O_3\rangle$ unit cells,[41] it then follows that, for the three $\langle Al\rangle$-$\langle \gamma\text{-}Al_2O_3\rangle$ interfaces concerned, the atomic density of oxygen of $\langle \gamma\text{-}Al_2O_3\rangle$ at the interface is equal to the atomic density of Al atoms of the $\langle Al\rangle$ substrate at the interface, and consequently $A_{\langle O\rangle}=A_{\langle Al\rangle}$. Expressions for the calculation of the molar interface area $A_{\langle Al\rangle}$ (and thus of $A_{\langle O\rangle}$) are given in Table I.

Values for both the interaction contribution and the mismatch contribution to the energy of the crystalline-crystalline $\langle Al\rangle$-$\langle \gamma\text{-}Al_2O_3\rangle$ interface and the resulting value of the interfacial energy $\gamma_{\langle Al\rangle\text{-}\langle \gamma\text{-}Al_2O_3\rangle}$ are presented in Table III for the three crystallographic faces of $\langle Al\rangle$ considered. Note that the calculated values of the mismatch energy and thus the interfacial energy $\gamma_{\langle Al\rangle\text{-}\langle \gamma\text{-}Al_2O_3\rangle}$ in Table III apply to the temperature at which the oxide film has been grown. For an oxide-film thickness $h_{\langle \gamma\text{-}Al_2O_3\rangle}<5$ nm, the value of $\gamma_{\langle Al\rangle\text{-}\langle \gamma\text{-}Al_2O_3\rangle}$ is dominated by the large negative contribution of the interaction energy, implying $\gamma_{\langle Al\rangle\text{-}\langle \gamma\text{-}Al_2O_3\rangle}<0$. It is noted that for oxide-film thickness $h_{\langle \gamma\text{-}Al_2O_3\rangle}>5$ nm the positive contribution of the mismatch energy becomes dominant, and $\gamma_{\langle Al\rangle\text{-}\langle \gamma\text{-}Al_2O_3\rangle}$ can become positive.

The coefficient of linear thermal expansion of $\langle Al \rangle$ is approximately ten times larger than that of $\langle \gamma\text{-}Al_2O_3 \rangle$ (see Table I), and therefore the growth mismatch f [cf. Eq. (15)] increases, virtually linearly, with increasing *growth* temperature T from 0.022 at $T_0 = 298.15\,K$ to 0.035 at $T = 900\,K$. Consequently, the (positive) mismatch contribution and thus the interfacial energy $\gamma_{\langle Al \rangle\text{-}\langle \gamma\text{-}Al_2O_3 \rangle}$ increases with increasing growth temperature. For most metal-substrate oxide-film systems, the coefficient of linear thermal expansion of the metal substrate is larger than that of the oxide film. Hence it can be concluded that for the general case of a $\langle MO_x \rangle$ film as formed by epitaxial growth on its substrate $\langle M \rangle$, the crystalline-crystalline $\langle M \rangle$-$\langle MO_x \rangle$ interface will be less stable for increasing growth temperature if the growth mismatch $f > 0$. Note that this temperature dependence will be reversed (i.e., the $\langle M \rangle$-$\langle MO_x \rangle$ interfacial energy decreases for increasing growth temperature) for metal-oxide systems with a growth mismatch $f < 0$.

In contrast with the mismatch energy, the Al-O interaction energy depends on the orientation of the $\langle Al \rangle$ substrate: the *smaller* the molar interface area $A_{\langle O \rangle}$ of oxygen at the $\langle Al \rangle$-$\langle \gamma\text{-}Al_2O_3 \rangle$ interface, the larger the Al-O interaction energy per unit area of the interface [cf. Eq. (12)] and thus the *lower* the resulting value of $\gamma_{\langle Al \rangle\text{-}\langle \gamma\text{-}Al_2O_3 \rangle}$ (see Table III). Since the value of $A_{\langle O \rangle}$ is equal to the molar interface area $A_{\langle Al \rangle}$ of Al atoms of the $\langle Al \rangle$ substrate at the interface (see above), it follows that the lowest interfacial energy $\gamma_{\langle Al \rangle\text{-}\langle \gamma\text{-}Al_2O_3 \rangle}$ occurs for the most densely packed plane of $\langle Al \rangle$ at the interface, i.e., the {111} plane (see Table III).

It can be concluded that, in contrast with the crystalline-amorphous interfacial energy $\gamma_{\langle Al \rangle\text{-}\{Al_2O_3\}}$, the crystalline-crystalline interfacial energy $\gamma_{\langle Al \rangle\text{-}\langle \gamma\text{-}Al_2O_3 \rangle}$ does depend on oxide-film thickness, the growth temperature, and the crystallographic orientation of the $\langle Al \rangle$ substrate (cf. Tables II and III).

In Ref. 56, the epitaxial interface between the {111} crystallographic plane of Nb and the {0001} crystallographic plane of $\alpha\text{-}Al_2O_3$ was modeled using an atomistic, static lattice simulation technique. Neglecting the mismatch of $f = 0.019$ between the lattices of the two phases at the $\langle Nb \rangle$-$\langle \alpha\text{-}Al_2O_3 \rangle$ interface, an interfacial energy of $\gamma_{\langle Nb \rangle\text{-}\langle \alpha\text{-}Al_2O_3 \rangle} = -3.61\,J\,m^{-2}$ was obtained.[56] This value is of the same magnitude as the values of the interfacial energies, calculated using Eq. (12) in Sec. III B 1, for the three $\langle Al \rangle$-$\langle \gamma\text{-}Al_2O_3 \rangle$ interfaces with $\gamma^{\text{mismatch}}_{\langle Al \rangle\text{-}\langle \gamma\text{-}Al_2O_3 \rangle} = 0$ at T_o, i.e., -4.387, -2.690, and $-3.799\,J\,m^{-2}$ for a $\langle \gamma\text{-}Al_2O_3 \rangle$ film on the {111}, {110}, and {100} crystallographic faces of $\langle Al \rangle$, respectively. Hence it may be concluded that the values obtained in this work for the interfacial energies $\gamma_{\langle Al \rangle\text{-}\{Al_2O_3\}}$ and $\gamma_{\langle Al \rangle\text{-}\langle \gamma\text{-}Al_2O_3 \rangle}$ are realistic (cf. Tables II and III).

The calculated difference between the interfacial energies $\gamma_{\langle Al \rangle\text{-}\{Al_2O_3\}}$ and $\gamma_{\langle Al \rangle\text{-}\langle \gamma\text{-}Al_2O_3 \rangle}$ per unit area of the $\langle Al \rangle$-$\{Al_2O_3\}$ interface [cf. Eq. (5)], i.e., $\gamma_{\langle Al \rangle\text{-}\{Al_2O_3\}} - \chi\gamma_{\langle Al \rangle\text{-}\langle \gamma\text{-}Al_2O_3 \rangle}$, at T_0, is plotted in Fig. 4 as a function of oxide-film thickness for the three crystallographic faces of $\langle Al \rangle$ considered. The dependence of the interfacial energy difference on the oxide-film growth temperature is shown in Fig. 5 for oxide films of variable thickness on a {100} Al substrate (similar results have been obtained for {110} and {111} $\langle Al \rangle$ substrates). Note that for a given thickness $h_{\{Al_2O_3\}}$ of the amorphous $\{Al_2O_3\}$ film, the thickness $h_{\langle \gamma\text{-}Al_2O_3 \rangle}$ of the *corresponding* epitaxial $\langle \gamma\text{-}Al_2O_3 \rangle$ film (cf. Sec. II) differs somewhat from $h_{\{Al_2O_3\}}$ due to both the difference in molar volumes of $\{Al_2O_3\}$ and $\langle \gamma\text{-}Al_2O_3 \rangle$, and the occurrence of mismatch strain (see the Appendix).

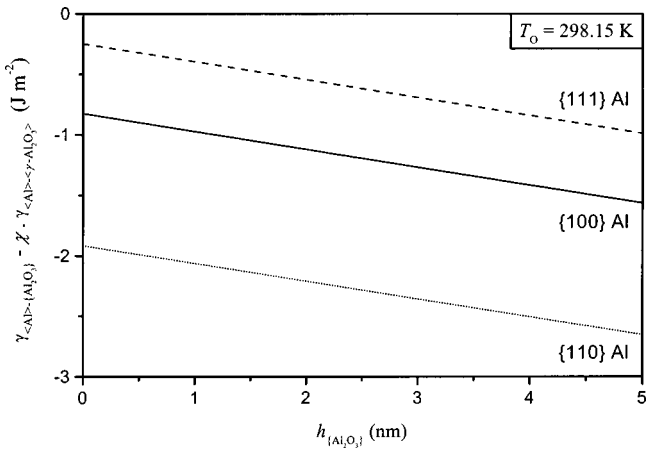

FIG. 4. Difference in the interfacial energy of the metal-substrate oxide-film interface of the amorphous $\{Al_2O_3\}$ cell and the corresponding crystalline $\langle \gamma\text{-}Al_2O_3 \rangle$ cell per unit area of the $\langle Al \rangle$-$\{Al_2O_3\}$ interface [cf. Eq. (5)] at $T_0 = 298.15\,K$ as a function of the thickness $h_{\{Al_2O_3\}}$ of the $\{Al_2O_3\}$ film (cf. Fig. 1 in Sec. II). Results are shown for Al_2O_3 films on {111}, {110}, and {100} Al substrates.

It follows that the $\langle Al \rangle$-$\{Al_2O_3\}$ interface is more stable than the corresponding $\langle Al \rangle$-$\langle \gamma\text{-}Al_2O_3 \rangle$ interface for all three crystallographic orientations of the $\langle Al \rangle$ substrate, even if $h_{\{Al_2O_3\}} \to 0$ (i.e., when the mismatch energy contribution is zero). Since the growth mismatch $f > 0$, the $\langle Al \rangle$-$\{Al_2O_3\}$ interface becomes more stable with respect to the corresponding $\langle Al \rangle$-$\langle \gamma\text{-}Al_2O_3 \rangle$ interface at higher growth temperature, in accordance with the above discussion.

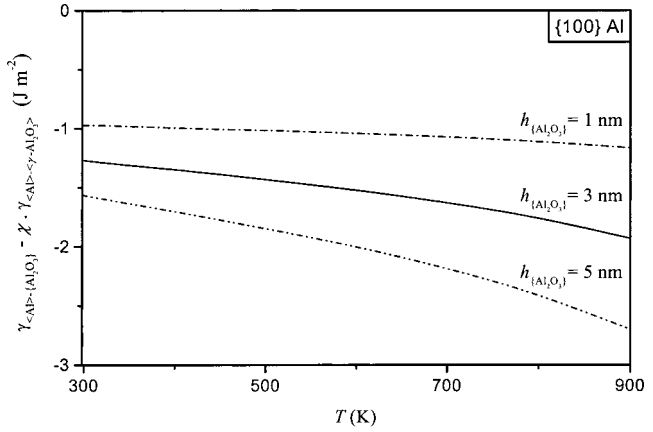

FIG. 5. Difference in interfacial energy of the metal-substrate oxide-film interface of the amorphous $\{Al_2O_3\}$ cell and the corresponding crystalline $\langle \gamma\text{-}Al_2O_3 \rangle$ cell per unit area of the $\langle Al \rangle$-$\{Al_2O_3\}$ interface [cf. Eq. (5)] as a function of the growth temperature T for an $\{Al_2O_3\}$ film of variable thickness $h_{\{Al_2O_3\}}$ on a {100} Al substrate.

V. STABILITY OF AMORPHOUS ALUMINUM-OXIDE FILMS ON CRYSTALLINE ALUMINUM SUBSTRATES

An amorphous $\{Al_2O_3\}$ film of thickness $h_{\{Al_2O_3\}}$ on an $\langle Al\rangle$ substrate will be more stable than a crystalline $\langle \gamma\text{-}Al_2O_3\rangle$ film of corresponding thickness $h_{\langle \gamma\text{-}Al_2O_3\rangle}$ on the same substrate if $\Delta G = G_{am} - G_{cryst} < 0$ (see Sec. II). For sufficiently thick oxide films, the bulk energy contribution dominates for the total energy of the metal oxide system. Thus, a critical thickness $h^{critical}_{\{Al_2O_3\}}$ can be defined as the oxide-film thickness of the $\{Al_2O_3\}$ cell for which $\Delta G = G_{am} - G_{cryst} = 0$; for $h_{\{Al_2O_3\}} < h^{critical}_{\{Al_2O_3\}}$, the stable oxide film is the amorphous one. It follows from Eq. (5) using Eqs. (11), (13d), and (A4), that

$$h^{critcal}_{\{Al_2O_3\}} = \frac{[\chi(\gamma_{\langle \gamma-Al_2O_3\rangle\text{-vac}} + \gamma^{interaction}_{\langle Al\rangle-\langle \gamma-Al_2O_3\rangle}) - \gamma_{\{Al_2O_3\}\text{-vac}} - \gamma_{\langle Al\rangle-\{Al_2O_3\}}]}{\left[\frac{\Delta G^f_{\{Al_2O_3\}} - \Delta G^f_{\langle \gamma-Al_2O_3\rangle}}{V_{\{Al_2O_3\}}} - \chi\xi\left(\frac{E}{1-\nu}\right)f^2\right]}, \tag{16}$$

where the ratio χ between the surface areas and the ratio ξ between the oxide film thicknesses of the $\{Al_2O_3\}$ and the $\langle \gamma\text{-}Al_2O_3\rangle$ cell (as formed by epitaxial growth) are obtained from Eqs. (A2) and (A4) in the Appendix, respectively. Note that $\Omega_{\{Al_2O_3\}} = 1$ [Eq. (5) of Sec. II; see Sec. III A and Ref. 26].

The value of $h^{critical}_{\{Al_2O_3\}}$, calculated by application of Eq. (16) using the results for the bulk, surface, and interfacial energies presented in Sec. IV, has been plotted in Fig. 6 as a function of the growth temperature T for an oxide film on the {111}, {110}, and {100} crystallographic faces of $\langle Al\rangle$: the amorphous oxide film is stable up to a thickness of 0.25, 4.08, and 2.13 nm at $T_0 = 298.15$ K, and up to a thickness of 0.44, 7.11, and 3.52 nm at $T = 900$ K, respectively (see Fig. 6).

The increased stability of the amorphous $\{Al_2O_3\}$ film for increasing growth temperature is the result of both (i) the *decrease* of the bulk Gibbs free-energy difference between the $\{Al_2O_3\}$ and the $\langle \gamma\text{-}Al_2O_3\rangle$ film with increasing growth temperature (cf. Fig. 2); and (ii) the *increase* of the crystalline-crystalline $\langle Al\rangle$-$\langle \gamma\text{-}Al_2O_3\rangle$ interfacial energy with increasing growth temperature (being more pronounced for thicker oxide films; cf. Fig. 5). Note that this temperature dependence may be much weaker or even of reversed nature for metal-oxide systems $\langle MO_x\rangle$ with a growth mismatch $f < 0$, because then the interfacial energy $\gamma_{\langle M\rangle\text{-}\langle MO_x\rangle}$ decreases with increasing growth temperature (see Sec. IV C).

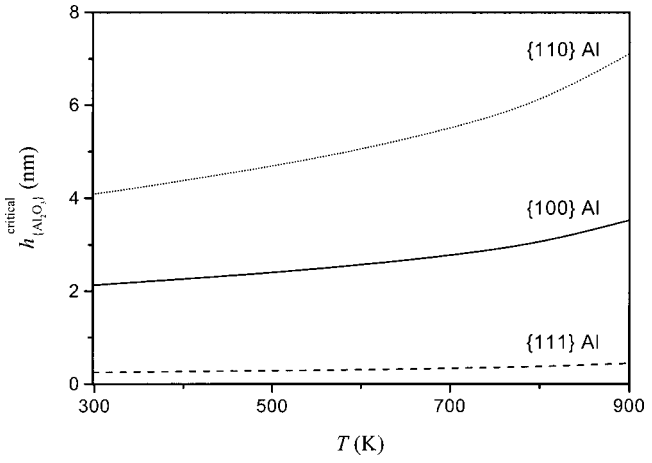

FIG. 6. The critical thickness $h^{critical}_{\{Al_2O_3\}}$, up to which an amorphous $\{Al_2O_3\}$ film instead of a crystalline $\langle \gamma\text{-}Al_2O_3\rangle$ film is preferred on the $\langle Al\rangle$ metal substrate, as a function of growth temperature *T*. Results are shown for Al_2O_3 films on {111}, {110} and {100} Al substrates.

Clearly, for the most densely packed crystallographic face of Al, i.e., the {111} face, the critical thickness is about 1–2 ''oxide monolayers'' (1 ML$\cong \frac{1}{4} a^0_{\langle \gamma\text{-}Al_2O_3\rangle} \cong 0.2$ nm; cf. Ref. 41), approximately independent of the growth temperature. Thus, after the very first stage of oxygen chemisorption and oxide formation, oxide-film growth on a {111} Al substrate is predicted to proceed by the direct formation and epitaxial growth of $\gamma\text{-}Al_2O_3$. For growth of an oxide film on the more ''open'' {110} and the {100} crystallographic faces of Al, preferred initial formation of an amorphous $\{Al_2O_3\}$ film is predicted, up to a critical oxide-film thickness $h^{critical}_{\{Al_2O_3\}}$ of 4.08 and 2.13 nm at $T_0 = 298.15$ K, respectively. This difference in the stability of an $\{Al_2O_3\}$ film, on the three different crystallographic faces of $\langle Al\rangle$, is directly related to the differences in both surface and interfacial energy of the corresponding $\langle \gamma\text{-}Al_2O_3\rangle$ film on the three different $\langle Al\rangle$ substrates (cf. Figs. 3 and 4 with Fig. 6).

As follows from Figs. 2, 3, and 4, for thin $\{Al_2O_3\}$ films (i.e., $h_{\{Al_2O_3\}} < 3$ nm) on {100} and {110} $\langle Al\rangle$ substrates at a growth temperature $T_0 = 298.15$ K, the difference in bulk Gibbs free energy between $\{Al_2O_3\}$ and $\langle \gamma\text{-}Al_2O_3\rangle$ is compensated for by about equally large corresponding differences in surface energy and interfacial energy, whereas at higher growth temperatures and for thicker oxide films the difference in interfacial energy becomes dominant. Further, the surface energy of (anhydrous) $\gamma\text{-}Al_2O_3$ is lowered upon chemisorption of H_2O.[52] Hence the chance of initial formation of a crystalline $\langle \gamma\text{-}Al_2O_3\rangle$ film on an $\langle Al\rangle$ substrate is enhanced by the presence of small amounts of water vapor.

Since the effect of pressure (within the range of, say, UHV up to 1 MPa) on the bulk and surface energies of $\{Al_2O_3\}$ and $\langle \gamma\text{-}Al_2O_3\rangle$ is approximately the same, the effect of pressure on the *difference* in bulk and surface energies [cf. Eq. (5)] can be neglected. Moreover, the effect of pressure on the enthalpy and entropy (per molar volume) of the solid phases is small, because the coefficient of volume expansion

β of solid phases is small ($\beta = 10^{-5} - 10^{-4}\,K^{-1}$) (see Ref. 57), and approximately the same for both $\{Al_2O_3\}$ and $\langle \gamma\text{-}Al_2O_3\rangle$. The energy of the $\langle Al\rangle$-$\langle \gamma\text{-}Al_2O_3\rangle$ interface [cf. Eq. (14)] depends on the growth mismatch f and the Poisson ratio and Young's modulus of $\langle \gamma\text{-}Al_2O_3\rangle$, which are nearly independent of pressure due to the high compressibility of the solid phases (i.e., $\sim 10^{11}$ Pa). Thus it can be concluded that the stability of an $\{Al_2O_3\}$ film on an $\langle Al\rangle$ substrate (i.e., the value of $h^{\text{critical}}_{\{Al_2O_3\}}$) is virtually independent of pressure.

The predictions obtained in this work on the thermodynamic stability of an amorphous $\{Al_2O_3\}$ film on the different crystallographic faces of $\langle Al\rangle$ may be compared with available transmission electron microscopy (TEM) observations of the developing microstructure of Al_2O_3 films on Al substrates. Unfortunately, for most of the TEM analyses reported (e.g., Refs. 1, 19, and 58), a 2–3 nm thick native oxide film was already present on the Al surface before heating and subsequent oxidation. Oxidation of the *bare* {100} and {110} crystallographic faces of Al up to temperatures of 823 K and an oxygen pressure $p_{O_2} = 1.33 \times 10^{-3}$ Pa, was shown to lead to the formation of an amorphous $\{Al_2O_3\}$ film,[18] as predicted by the results shown in Fig. 6; after a long period of annealing (>60 h) at 823 K and $p_{O_2} = 1.33 \times 10^{-3}$ Pa, nucleation and growth of $\gamma\text{-}Al_2O_3$ was observed.[18] The oxidation of a *bare* {111} Al substrate at 773 K and $p_{O_2} = 2.67 \times 10^{-5}$ Pa, was observed to occur by the direct formation and *outward* growth of $\gamma\text{-}Al_2O_3$ islands and the development of an amorphous oxide was not observed.[17] Indeed, the corresponding critical thickness $h^{\text{critical}}_{\{Al_2O_3\}}$ is predicted to be very small (Fig. 6).

Knowledge on the thermodynamic stability of amorphous oxide films on their metal (or semiconductor)[10] substrates is a prerequisite for technological applications where the formation of a stable thin amorphous oxide film with uniform thickness on the substrate is desired: for example, to realize passivation of metals and semiconductors and to establish diffusion barriers in solid state devices (e.g., tunnel junctions). The absence of grain boundaries and other lattice defects in the amorphous oxide reduce ionic migration through the oxide,[2,3,23] improve electronic properties (e.g., high dielectric strength and low leakage current) and increase corrosion resistance.[2,3,5,23] Moreover, due to the relatively large free volume[21,22] and the bond flexibility[2,23] of the amorphous oxides, a mismatch with their substrates can be accommodated by viscous flow,[2,21–26] thereby promoting strong adhesion across the substrate-film interface.[2,3,5,23]

VI. CONCLUSIONS

(i) The energy of the interface between a crystalline metal $\langle M\rangle$ and its oxide MO_x is generally smaller for the amorphous oxide $\{MO_x\}$ than for the crystalline oxide $\langle MO_x\rangle$.

(ii) For sufficiently thin oxide films on a metal substrate $\langle M\rangle$, the amorphous state can be preferred over the crystalline state, because the higher bulk energy of the amorphous oxide film $\{MO_x\}$, as compared to the corresponding crystalline oxide film $\langle MO_x\rangle$, can be overcompensated for by the relatively low sum of the $\{MO_x\}$ surface energy and $\langle M\rangle$-$\{MO_x\}$ interfacial energy.

(iii) Adopting a ''macroscopic atom'' approach,[11,13–16] thermodynamic parameters for a description of interfacial energies of metal metal-oxide systems can be well assessed.

(iv) By calculating the total energy of the metal-substrate metal-oxide film system, i.e., including Gibbs energies of formation, mismatch energy, and interfacial and surface energies, a critical thickness of the oxide film can be calculated up to which the amorphous oxide is thermodynamically more stable than the corresponding crystalline oxide.

(v) The difference in thermodynamic stability of an amorphous $\{MO_x\}$ film on its metal substrate $\langle M\rangle$ (with respect to the corresponding epitaxial $\langle MO_x\rangle$ film on the same substrate) as a function of *growth temperature* is governed by (i) the decrease of the bulk Gibbs free energy difference between the $\{MO_x\}$ and the $\langle MO_x\rangle$ film with increasing growth temperature, and (ii) the change of the growth mismatch between the lattices of $\langle MO_x\rangle$ and $\langle M\rangle$ at the interface with increasing growth temperature. In most cases, where a tensile growth stress occurs in the crystalline oxide film parallel to the interface and the thermal expansion coefficient of the metal substrate is larger than that of the oxide, the amorphous $\{MO_x\}$ film on the $\langle M\rangle$ substrate will be more stable with respect to the corresponding epitaxial $\langle MO_x\rangle$ film at higher growth temperatures; the reverse can be true in the case of a compressive growth stress.

(vi) The differences in the relative stability of an amorphous $\{MO_x\}$ film on *different crystallographic faces* of the $\langle M\rangle$ substrate are caused by the differences in the crystalline-crystalline $\langle M\rangle$-$\langle MO_x\rangle$ interfacial energy. Formation of a crystalline oxide is more likely for a more densely packed crystallographic face of the $\langle M\rangle$ substrate.

(vii) The predicted stabilities for an amorphous $\{Al_2O_3\}$ film on a $\langle Al\rangle$ substrate agree well with previous transmission electron microscopy observations: amorphous Al_2O_3 develops on {100} Al and {110} Al, and crystalline $\gamma\text{-}Al_2O_3$ develops on {111} Al.

ACKNOWLEDGMENTS

Financial support by the Foundation for Fundamental Research of Matter (FOM) is gratefully acknowledged. The authors are grateful to Dr. A. J. Böttger for helpful discussions on the estimation of interfacial energies.

APPENDIX

For a thin crystalline $\langle \gamma\text{-}Al_2O_3\rangle$ film formed by epitaxial growth on the {111}, {110} or {100} crystallographic faces of an $\langle Al\rangle$ substrate, the tensile strain $\varepsilon_{\parallel}$ at the growth temperature is (i) independent of the direction within the plane parallel to the $\langle Al\rangle$-$\langle \gamma\text{-}Al_2O_3\rangle$ interface, (ii) the same for the three interfaces considered, and (iii) equal to the growth mismatch f [see the discussion above Eq. (15) in Sec. IV C].

Then the width and length $l_{\langle \gamma\text{-}Al_2O_3\rangle}$ of the accordingly strained $\langle \gamma\text{-}Al_2O_3\rangle$ cell on the $\langle Al\rangle$ substrate [cf. Fig. 1(b)] are related to the width and length of the unstrained $\langle \gamma\text{-}Al_2O_3\rangle$ cell, $l^{\text{unstr}}_{\langle \gamma\text{-}Al_2O_3\rangle}$, by (cf. Secs. II and III B 2)

$$l_{\langle \gamma - Al_2O_3\rangle} = l^{\text{unstr}}_{\langle \gamma - Al_2O_3\rangle}(1+f). \tag{A1}$$

The corresponding amorphous $\{Al_2O_3\}$ cell (cf. Fig. 1(a) in Sec. II) is unstrained, as discussed below Eq. (6) in Sec. III A (cf. Ref. 44). It then follows that the ratio χ in Eq. (4b) in Sec. II between the surface areas of the $\{Al_2O_3\}$ and $\langle\gamma\text{-}Al_2O_3\rangle$ cells is related to the molar volumes $V_{\{Al_2O_3\}}$ and $V_{\langle\gamma\text{-}Al_2O_3\rangle}$ of $\{Al_2O_3\}$ and unstrained $\langle\gamma\text{-}Al_2O_3\rangle$ according to

$$\chi=\left(\frac{l_{\langle\gamma-Al_2O_3\rangle}}{l_{\{Al_2O_3\}}}\right)^2=\left(\frac{l^{\rm unstr}_{\langle\gamma-Al_2O_3\rangle}(1+f)}{l_{\{Al_2O_3\}}}\right)^2$$
$$=\left(\frac{V_{\langle\gamma-Al_2O_3\rangle}}{V_{\{Al_2O_3\}}}\right)^{2/3}(1+f)^2. \quad \text{(A2)}$$

The thickness $h_{\langle\gamma\text{-}Al_2O_3\rangle}$ of the strained $\langle\gamma\text{-}Al_2O_3\rangle$ film is related to the thickness $h^{\rm unstr}_{\langle\gamma\text{-}Al_2O_3\rangle}$ of the corresponding unstrained $\langle\gamma\text{-}Al_2O_3\rangle$ cell by [cf. Eq. (A1)]

$$h_{\langle\gamma-Al_2O_3\rangle}=h^{\rm unstr}_{\langle\gamma-Al_2O_3\rangle}(1-2\nu f), \quad \text{(A3)}$$

where ν denotes the Poisson ratio of $\langle\gamma\text{-}Al_2O_3\rangle$. Thus the ratio ξ of the heights of the strained $\langle\gamma\text{-}Al_2O_3\rangle$ cell and the corresponding unstrained $\{Al_2O_3\}$ cell is related to the molar volumes $V_{\{Al_2O_3\}}$ and $V_{\langle\gamma\text{-}Al_2O_3\rangle}$ of the unstrained phases by [cf. Eq. (A2)]

$$\xi=\frac{h_{\langle\gamma-Al_2O_3\rangle}}{h_{\{Al_2O_3\}}}=\left(\frac{h^{\rm unstr}_{\langle\gamma-Al_2O_3\rangle}(1-2\nu f)}{h_{\{Al_2O_3\}}}\right)$$
$$=\left(\frac{V_{\langle\gamma-Al_2O_3\rangle}}{V_{\{Al_2O_3\}}}\right)^{1/3}(1-2\nu f). \quad \text{(A4)}$$

Using the data in Table I and the values of f as obtained from Eq. (15) in Sec. IV C, it follows that χ increases from 0.960 at $T_0(=298.15\,\text{K})$ to a value of 0.985 at 900 K, whereas ξ decreases from 0.949 at T_0 to 0.943 at 900 K.

*Electronic address: L. P. H. Jeurgens@tnw.tudelft.nl
†Electronic address: W.G.Sloof@tnw.tudelft.nl

[1] P. E. Doherty and R. S. Davis, J. Appl. Phys. **34**, 619 (1963).
[2] A. G. Reversz and F. P. Fehlner, Oxid. Met. **15**, 297 (1981).
[3] F. P. Fehlner, *Low-Temperature Oxidation: the Role of Vitreous Oxides* (Wiley-Interscience, New York, 1981).
[4] K. R. Lawless, Rep. Prog. Phys. **37**, 231 (1973).
[5] A. G. Revesz, Phys. Status Solidi **24**, 115 (1967); **19**, 193 (1967).
[6] H. M. Kennet and A. E. Lee, Surf. Sci. **48**, 633 (1975).
[7] J. V. Cathcart and G. F. Petersen, J. Electrochem. Soc. **115**, 595 (1968).
[8] T. M. Christensen, C. Raoul, and J. M. Blakely, Appl. Surf. Sci. **26**, 408 (1986).
[9] G. Rovida and M. Maglietta, in *Proceedings of the 7th International Vacuum Congress and 3rd International Conference on Solid Surfaces, Vienna, 1977*, edited by R. Dobrozemsky, F. Rüdenauer, F. P. Viehböck, and A. Breth (Berger & Söhne, Horn, 1977), p. 963.
[10] The thermodynamical model presented here for the case of thin metal-oxide films formed on their metal substrates is equally valid for thin oxide films formed on their semiconductor substrates (e.g., Si or Ge). Therefore, in this paper no distinction will be made between the two.
[11] R. Benedictus, A. Böttger, and E. J. Mittemeijer, Phys. Rev. B **54**, 9109 (1996).
[12] S. Blonski and S. H. Garofalini, Surf. Sci. **295**, 263 (1993).
[13] F. R. de Boer, R. Boom, W. C. M. Mattens, A. R. Miedema, and A. K. Niessen, *Cohesion in Metals: Transition Metals Alloys* (North-Holland, Amsterdam, 1989), Chaps. 2 and 4.
[14] A. R. Miedema and P. F. De Châtel, in *Theory of Alloy Phase Formation*, edited by L. H. Bennet (AIME, New Orleans, 1980), p. 344.
[15] A. R. Miedema, J. Less-Common Met. **32**, 117 (1973).
[16] A. R. Miedema and F. J. A. den Broeder, Z. Metallkd. **70**, 14 (1979).
[17] J. I. Eldridge, R. J. Hussey, D. F. Mitchell, and M. J. Graham, Oxid. Met. **30**, 301 (1988).
[18] K. Shinohara, T. Seo, and H. Kyogoku, Z. Metallkd. **73**, 774 (1982).
[19] K. Thomas and M. W. Roberts, J. Appl. Phys. **32**, 70 (1961).
[20] R. K. Hart and J. K. Maurin, Surf. Sci. **20**, 285 (1970).
[21] F. Spaepen, Acta Metall. **25**, 407 (1977).
[22] S. Sundaram and R. J. Clifton, Mech. Mater. **29**, 233 (1998).
[23] A. G. Revesz and J. Kruger, in *Passivity of Metals*, edited by R. P. Frankenthal and J. Kruger (Electrochemical Society, Princeton, 1978), p. 137.
[24] N. F. Mott, Philos. Mag. B **55**, 117 (1987).
[25] E. A. Irene, E. Tierney, and J. Angilello, J. Electrochem. Soc. **129**, 2594 (1982).
[26] J. S. Leach and P. Neufeld, Corros. Sci. **9**, 255 (1969).
[27] J. E. McDonald and J. G. Eberhart, Trans. Metall. Soc. AIME **233**, 512 (1965).
[28] D. Chatain, I. Rivollet, and N. Eustathopoulos, J. Chim. Phys. Phys.-Chim. Biol. **83**, 561 (1986); **84**, 201 (1987).
[29] M. W. Chase *et al.*, J. Phys. Chem. Ref. Data **9**, 156 (1998); M. W. Chase, Jr.. NIST-JANAF Thermochemical Tables 4th Ed., Part I. Al-Co (American Institute of Physics, New York, 1998), p. 156-159.
[30] T. Tokuda and H. Harada, in *Proceedings of the 2nd International Conference on the Properties of Liquid Metals, Tokyo, 1972*, edited by S. Takeuchi (Taylor & Francis, London, 1973), p. 583.
[31] O. Kubaschewski and C. B. Alcock, *Metallurgical Thermochemistry* (Pergamon, Oxford, 1979), p. 477.
[32] E. Fromm, O. Mayer, and W. Nickerson, Surf. Sci. **57**, 775 (1976).
[33] F. Spaepen, Acta Metall. **23**, 729 (1975).
[34] F. Spaepen and R. B. Meyer, Scr. Metall. **10**, 257 (1976).
[35] R. H. Ewing, Philos. Mag. **25**, 779 (1972).
[36] In this paper the actual molar interface area will be used instead of the commonly used approximation for the average molar interface area of a crystalline phase $\langle M\rangle$, i.e., $\overline{A}_{\langle M\rangle}=pC_0V^{2/3}_{\langle M\rangle}$, where C_0 is a constant depending on the shape of the Wigner-Seitz cell of M, and $V_{\langle M\rangle}$ denotes the molar volume of $\langle M\rangle$ (cf. Refs. 11 and 13–16).
[37] D. Turnbull, in *Impurities and Imperfections*, edited by O. T. Marzke (American Society of Metals, Cleveland, 1955), p. 121.
[38] J. N. Chirigos, in *Physical Metallurgy of Stress Corrosion Fracture*, edited by T. H. Rhodin (Interscience, New York, 1959), p. 70.

[39] Y. Ikuhara and P. Pirouz, Microsc. Res. Tech. **40**, 206 (1998).

[40] D. L. Smith, *Thin-Film Deposition: Principles and Practice* (McGraw-Hill, New York, 1995), Chap. 6.

[41] Aluminum metal has a fcc structure (space group $Fm\bar{3}m$) with a unit cell with an (unstrained) lattice parameter at $T_0 = 298.15$ K of $a^0_{\mathrm{Al}} = 4.0494$ Å (see Ref. 42). γ-Al_2O_3 has a defect cubic spinel structure (space group $Fd\bar{3}m$), with a unit cell with an unstrained lattice parameter $a^0_{\langle \gamma\text{-}Al_2O_3\rangle} = 7.924$ Å (see Ref. 43). The unit cell contains 32 oxygen anions in a $2\times2\times2$ array of fcc cells of the anion sublattice, and $21\frac{1}{3}$ aluminum cations divided over the octrahedral and tetrahedral interstices. Hence, using the given orientation relationship between the $\langle$Al$\rangle$ substrate and the thin epitaxial $\langle \gamma$-$Al_2O_3\rangle$ film [see above Eq. (15) in Sec. IV C], it follows, for the three $\langle$Al$\rangle$-$\langle \gamma Al_2O_3\rangle$ interfaces considered, that $a^{0,\mathrm{strained}}_{\langle \gamma\text{-}Al_2O_3\rangle} = 2\times a^0_{\langle \mathrm{Al}\rangle}$.

[42] Powder Diffraction file, 04-0787 from International Center for Diffraction Data (ICDD).

[43] Powder Diffraction file, 29-0063 from International Center for Diffraction Data (ICDD).

[44] J. R. Willis, S. C. Jain, and R. Bullough, Philos. Mag. A **62**, 115 (1990).

[45] J. H. van der Merwe, Surf. Sci. **31**, 198 (1972).

[46] For the calculation of the Gibbs free energy of formation of amorphous $\{Al_2O_3\}$ in this work, the heat capacity C^0_p of amorphous $\{Al_2O_3\}$ below the liquid-glass transition temperature at 1350 K was taken to be the same as that of γ-Al_2O_3 (see Ref. 29).

[47] E. A. Brandes and G. B. Brook, *Smithells Metals Reference Book* 7th Ed. (Butterworth-Heinemann, Oxford, 1992), p. 14-3.

[48] H. Yanagida and G. Yamaguchi, Bull. Chem. Soc. Jpn. **37**, 1229 (1964).

[49] W. J. Bernard and J. W. Cook, J. Electrochem. Soc. **106**, 643 (1959).

[50] M. R. Gallas and G. J. Piermarini, J. Am. Chem. Soc. **77**, 2917 (1994).

[51] X.-G. Wang, W. Weiss, Sh. K. Shaikhurdinov, M. Ritter, M. Petersen, F. Wagner, R. Schlögl, and M. Scheffler, Phys. Rev. Lett. **81**, 1038 (1998).

[52] J. M. McHale, A. Aroux, A. J. Perrotta, and A. Navrotsky, Science **277**, 788 (1997).

[53] F. Réti, I. Bertóti, and G. Mink, Solid State Ionics **44**, 33 (1990).

[54] Y. S. Anisimov, E. F. Grits, and B. S. Mitin, Izv. Akad. Nauk SSSR, Neorg. Mater. **13**, 1444 (1977) [Inorg. Mater. (Transl. of Neorg. Mater.) **13**, 1168 (1977)].

[55] In Refs. 19 and 20 an additional orientation relationship between γ-Al_2O_3 and the Al substrate was found for the {100} crystallographic face of Al.

[56] D. M. Duffy, J. H. Harding, and A. M. Stoneham, Acta Mater. **44**, 3293 (1996).

[57] The effect of pressure on enthalpy and entropy per molar volume can be estimated from (cf. Ref. 29) $V^{-1}(\partial H/\partial p)_T = (1-\beta T)$ and $V^{-1}(\partial S/\partial p)_T = -\beta$, where β is the coefficient of volume expansion.

[58] K. Shimizu, A. Gotoh, K. Kobayashi, G. E. Thompson, and G. C. Wood, in *Microscopy of Oxidation*, edited by M. J. Bennet and G. W. Lorimer (Institute of Metals, London, 1991), p. 144.